SI Appendix

SI Appendix, Table S1. Cryo-EM data collection and structure refinement statistics

	CMG-ssDNA (14 bases)	CMG-ssDNA (9 bases)	CMG-forked DNA
Data Collection			
EM equipment	FEI Titan Krios	FEI Titan Krios	FEI Titan Krios
Voltage (kV)	300	300	300
Detector	Gatan K2	Gatan K2	Gatan K2
Pixel size (Å)	1.3	1.3	1.3
Electron dose (e^-/Å^2)	50	50	50
Defocus range (μm)	1.5~3.5	1.5~3.5	1.5~3.5
3D Reconstruction			
Software	RELION 1.4	RELION 1.4	RELION 1.4 / 2.0
Final number of particles included	83,002	83,043	58,511
Resolution (Å)	4.9	6.2	6.1
B-factor sharpening (Å^2)	-149	-185	-152
Model composition			
Peptide chains	11		11
Protein residues	4989		4969
Nucleotides	3 (AMPPNP)		3 (ATP)
DNA bases	14		33
R.m.s deviations			
Bonds length (Å)	0.007		0.004
Bonds Angle (°)	1.327		0.926
Ramachandran plot			
Preferred (%)	89.0		90.2
Allowed (%)	10.0		8.8
Outlier (%)	1.0		1.0
Validation			
Molprobity score	3.34 (76%)		3.07 (86%)

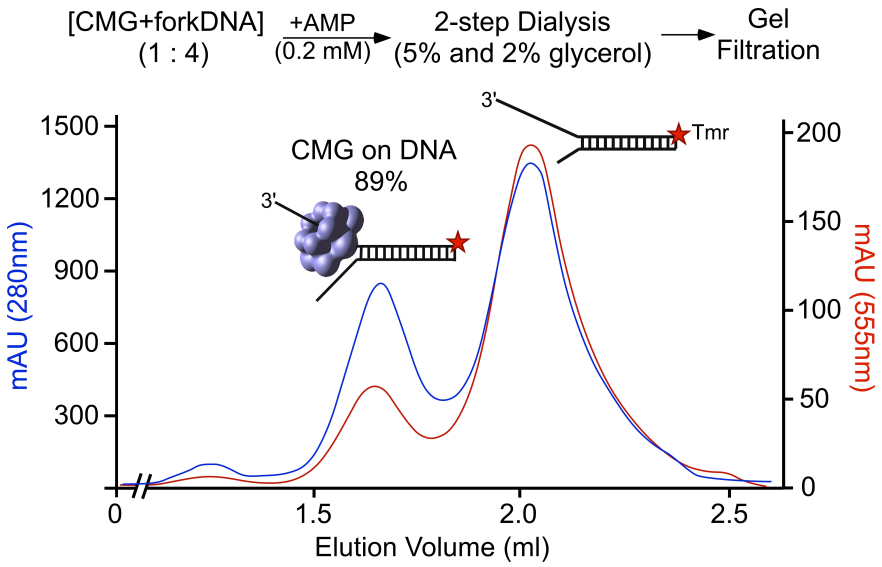

SI Appendix, Figure S1. Isolation of CMG-DNA complex by gel filtration. CMG was incubated with a 4 fold molar excess of fork DNA in the presence of 0.2 mM AMPPNP, then glycerol was removed in two dialysis steps before application to a 2.4 ml gel filtration column. Absorbances at 280 nm and 555 nm are shown. The fork contains a TAMRA chromophore (aaterisk), enabling the ability to follow the presence of the DNA. Peak fractions containing both DNA and protein were analyzed by SDS PAGE, and a peak fraction was used to make cryo grids. See Materials and Methods for details.

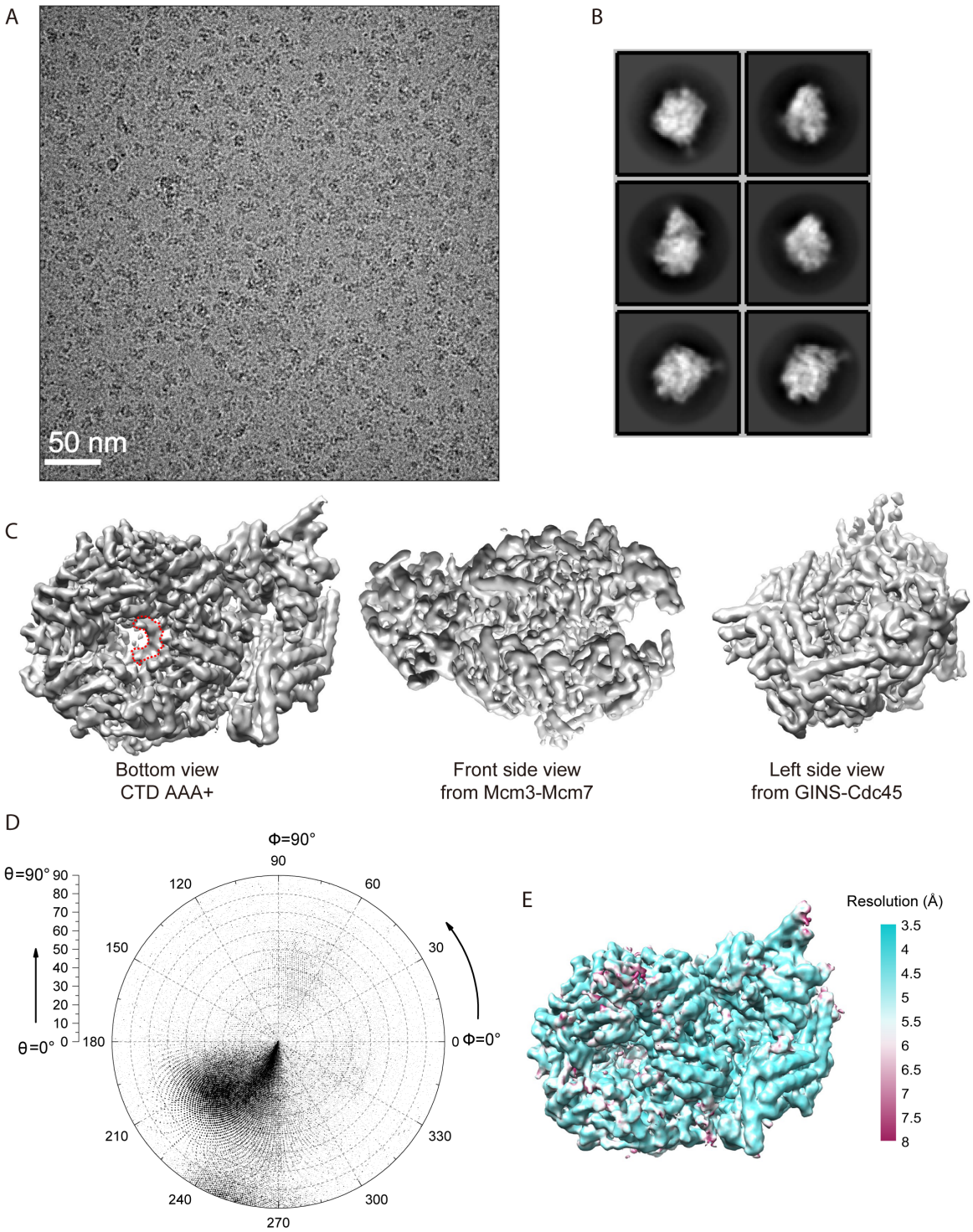

SI Appendix, Figure S2. Cryo-EM of the ScCMG bound to ssDNA in the presence of AMPPNP. (**A**) A representative motion-corrected raw electron micrograph. (**B**) Selected 2D class averages. (**C**) Three orthogonal views of the 4.9 Å resolution 3D map of CMG-ssDNA. (**D**) The Eulerian angle distribution of the CMG-ssDNA complex. The particles were preferentially oriented in side views, but virtually all orientations were present, such that the 3D map at 4.9 Å is of similar quality in all directions. (**E**) Local resolution map of the reconstructed CMG-DNA map showing the bottom C-tier AAA+ view.

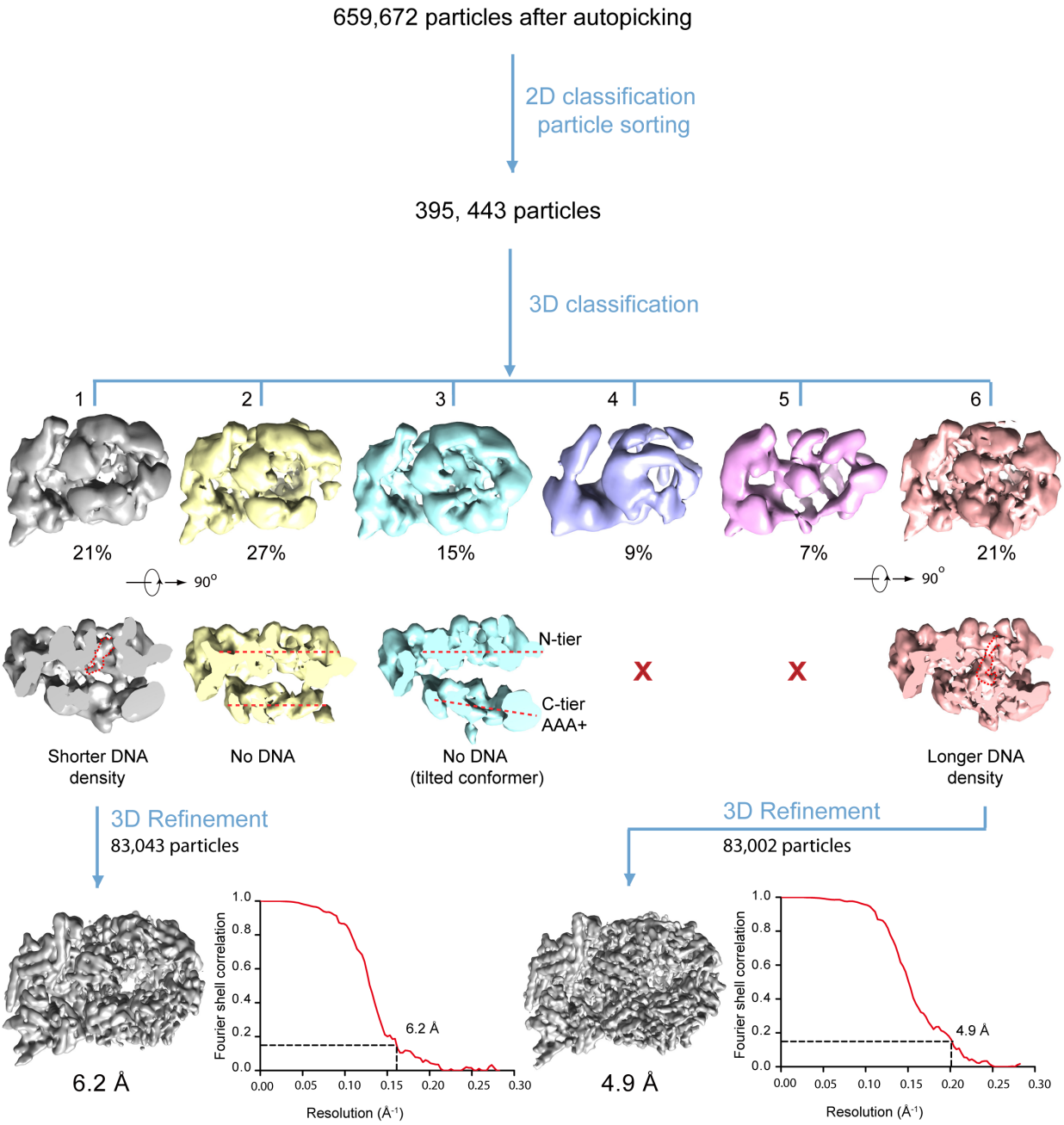

SI Appendix, Figure S3. A workflow of image processing and 3D reconstruction of CMG-ssDNA in the presence of AMPPNP. Out of six 3D classes, two classes had clear DNA densities (Classes #1 and #4). The two classes further refined to yield the reported 3D maps at 6.2 Å resolution (9-base nucleotides) and 4.9 Å resolution (14-base nucleotides), respectively, according to the gold standard Fourier shell correlation, shown to the right of the final 3D maps.

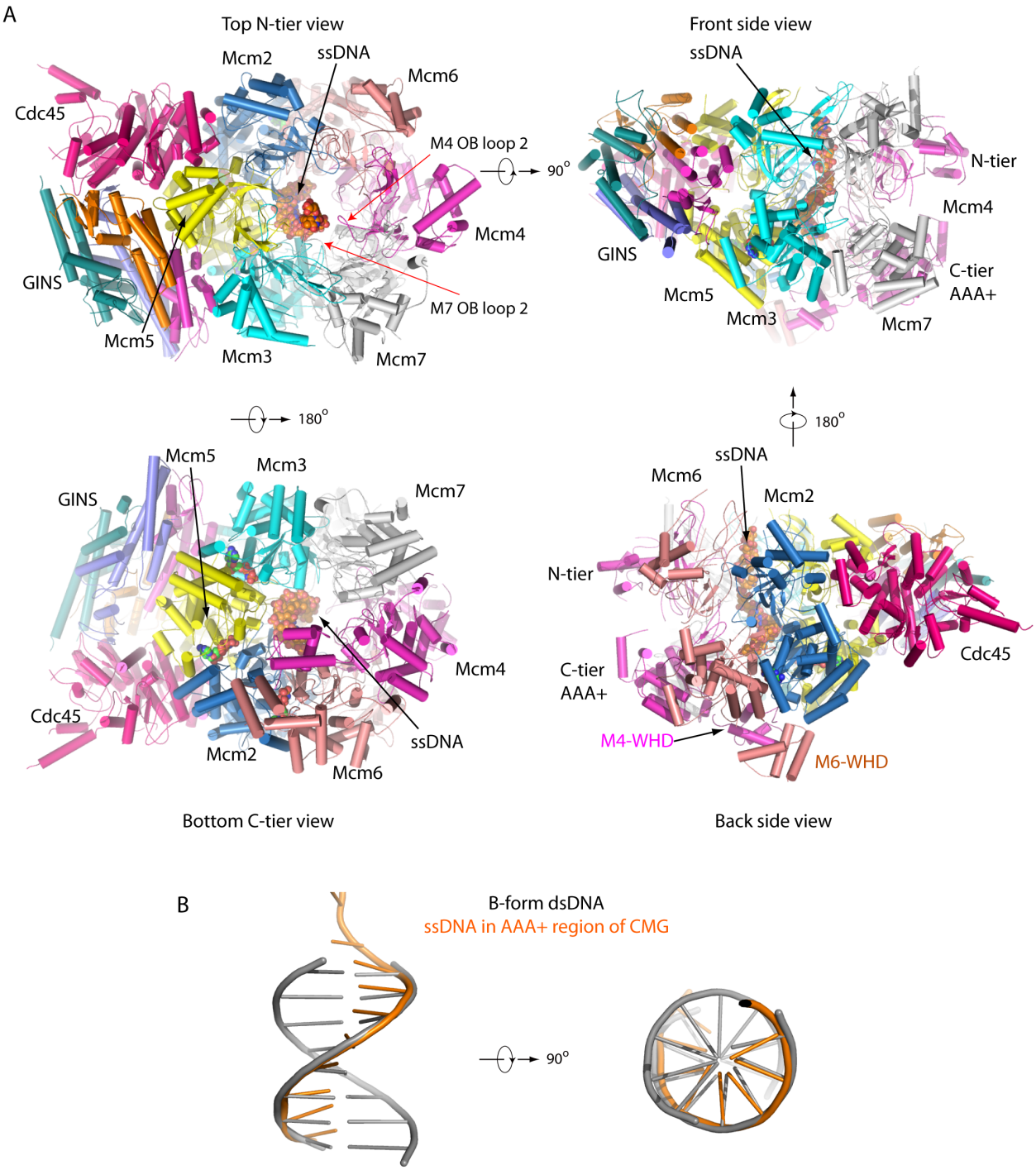

SI Appendix, Figure S4. Overall structure of CMG-ssDNA at 4.9 Å resolution. (A) The 14-base ssDNA binds to the interior surface of the N-tier ring channel, then extends to the C-tier AAA interior surface. The first panel shows that the OB loops 2 of Mcm4 (M4) and Mcm7 (M7) interact with the ssDNA inside the N-tier ring. (**B**) Alignment of last 8 base of the 14-base ssDNA (orange) with an ideal B-form dsDNA (grey).

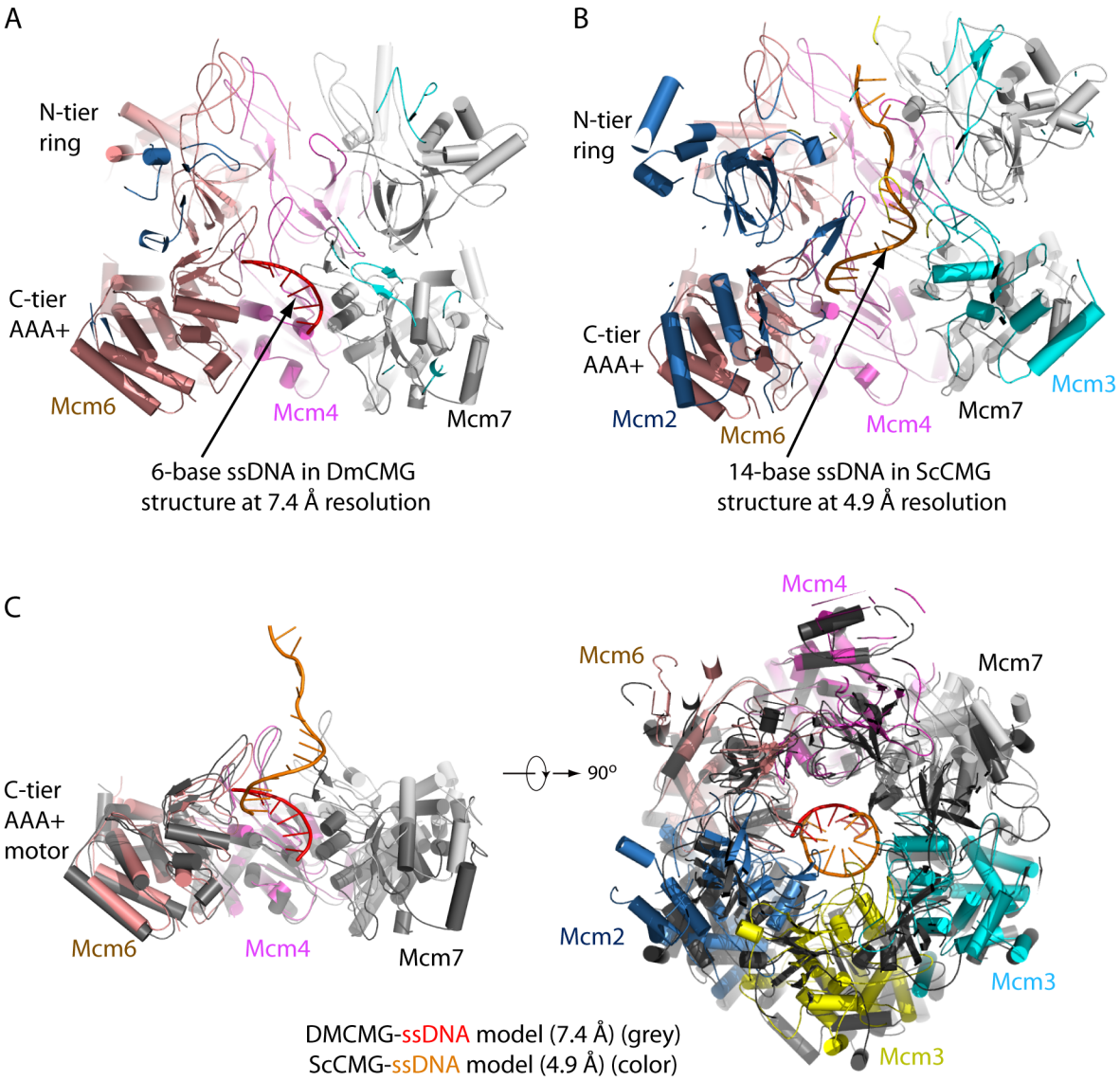

SI Appendix, Figure S5. Comparison of a previously reported 7.4 Å cryo-EM structure of D.m. CMG resolving 6-base ssDNA (EMD-3318) with our current 4.9 Å cryo-EM structure of S.c. CMG resolving 14-base ssDNA. (A) In the D.m. CMG-ATPγS-DNA model[1], a B-form ssDNA with length of 6 bp was identified to bind the CTDs of Mcm6, Mcm4, and Mcm7. (**B**) In our S.c. CMG-ssDNA structure, DNA binds to the CTDS of Mcm2, Mcm3, Mcm5, and Mcm6, but the CTDs of Mcm4 and Mcm7 are not involved in DNA binding. (**C**) Superimposition of S.c. CMG-ssDNA structure (color) and D.m. CMG-ATPγS-DNA model (Mcm2-7 in dark grey and DNA in red) by aligning CTDs of Mcm6 and Mcm4. CTDs of Mcm6 and Mcm4, but not of Mcm7, of the two structures aligned well. The ssDNA in these two models appear to belong to the same (leading) strand and are both in the B-form-like spiral. This observation indicates that CTDs of all six Mcm proteins bind the leading strand during translocation, but may be at a different stage of the nucleotide cycle.

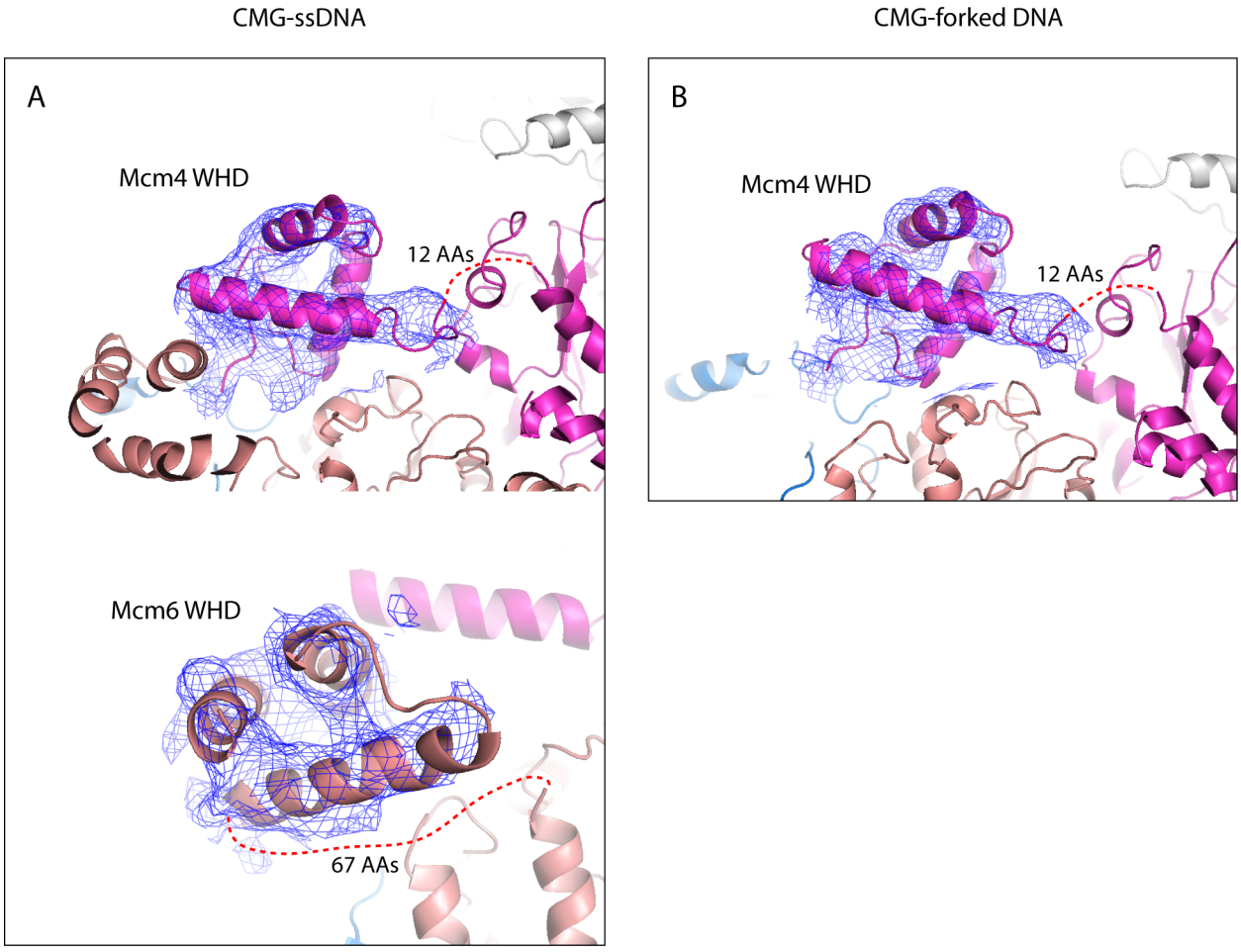

SI Appendix, Figure S6. Movement of Mcm4 and Mcm6 WHDs in DNA bound CMG structures as compared to the apo CMG structure. (**A**) Electron densities of WHDs of Mcm4 and Mcm6 in the CMG-ssDNA structure. (**B**) Electron density map of Mcm4 WHD in the CMG-forked DNA structure.

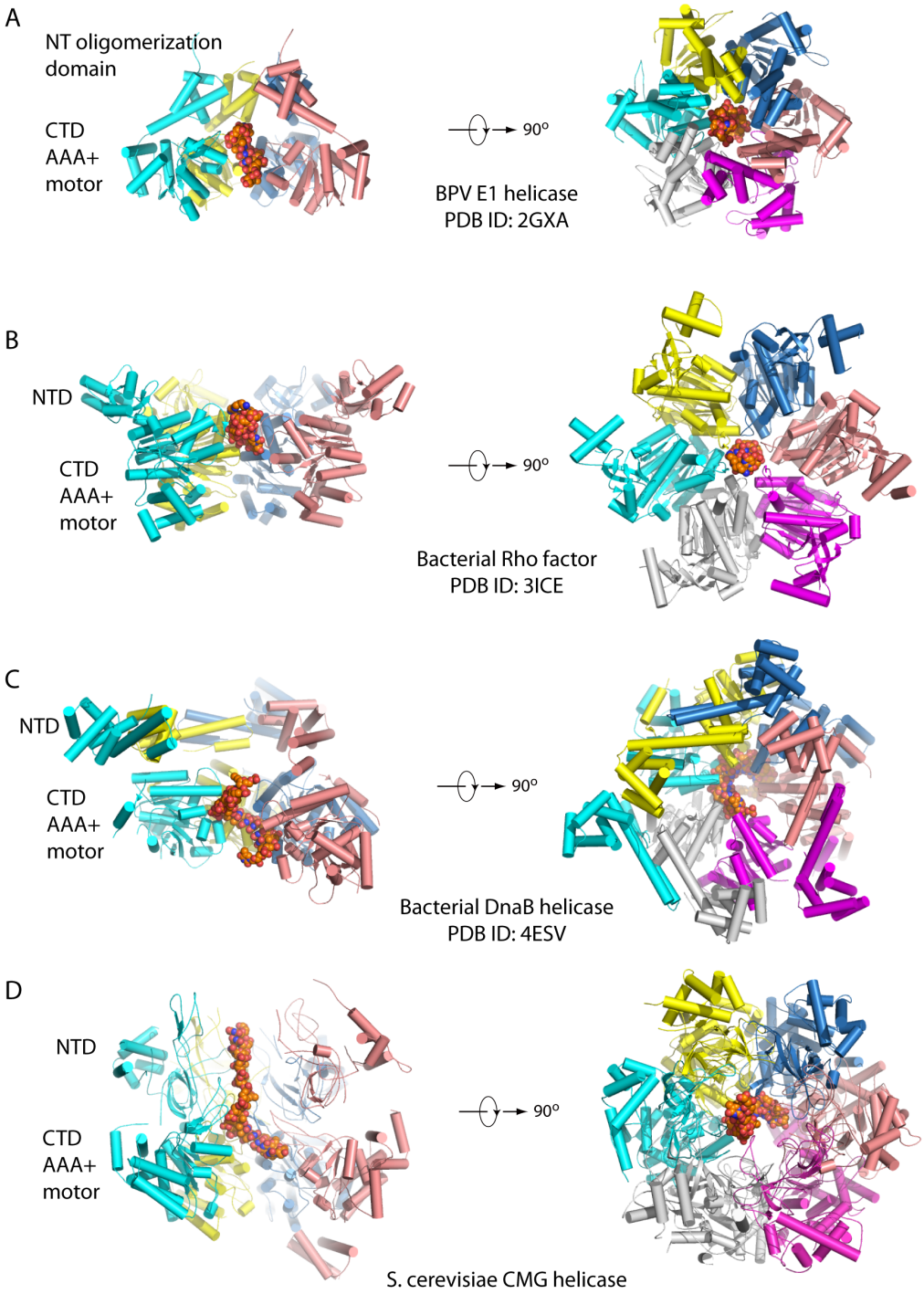

SI Appendix, Figure S7. Comparison of the crystal structures of four helicase motors in complex with ssDNA. (**A**) BPV E1 helicase[2]. (**B**) Bacterial Rho termination factor[3]. (**C**) Bacterial DnaB hexamer helicase[4]. (**D**) *S. cerevisiae* CMG helicase. In all panels, the side views (left images) are all shown with the 5' end of the DNA on top. Except for the current CMG that binds ssDNA at both N-tier and the C-tier motor ring, all other structures bind DNA only in their C-tier motor ring. Note that only ssDNA in the DnaB and the CMG are in the dsDNA-like B-form. The central channels of the E1 and the Rho hexamers are too small for the spiral ssDNA to form the dsDNA-like B-configuration.

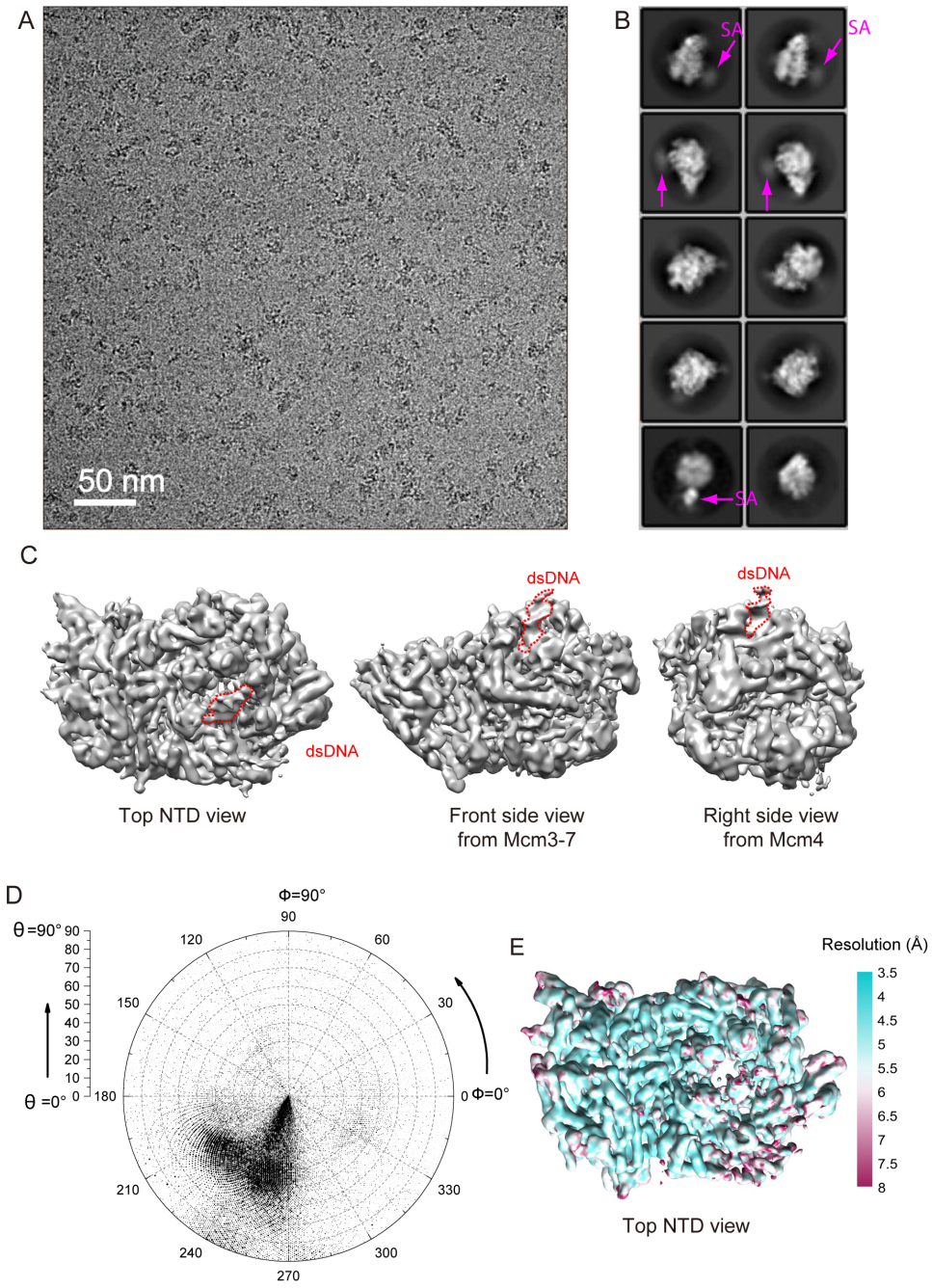

SI Appendix, Figure S8. Cryo-EM of the *S. cerevisiae* CMG trapped on a forked DNA by a dual biotin streptavidin block. (**A**) A representative motion-corrected raw electron micrograph. (**B**) Selected 2D class averages. The pink arrows point to streptavidin density (SA) at the N-tier ring side of the CMG structure. (**C**) Three orthogonal views of the 3D map of CMG-DNA-streptavidin. (**D**) The Eulerian angle distribution of the CMG-forked DNA complex. The particles were preferentially oriented in side views, most likely due to the presence of long forked DNA. But virtually all orientations were present, such that 3D map at 6.1 Å is of similar quality in all directions. (**E**) Local resolution map of the reconstructed CMG-DNA map showing the bottom C-tier AAA+ view.

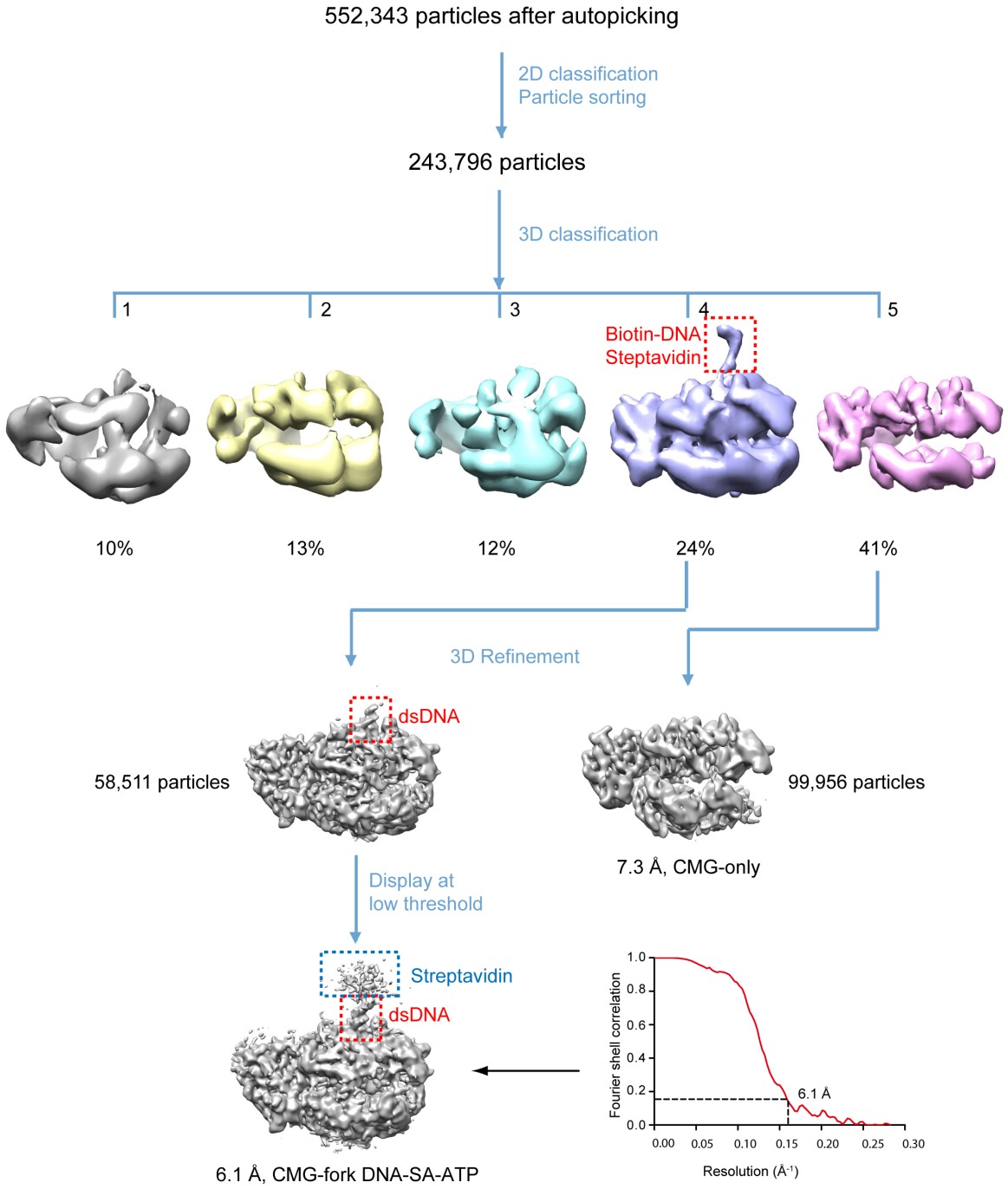

SI Appendix, Figure S9. A workflow of image processing and 3D reconstruction of streptavidin blocked CMG-forked DNA in the presence of ATP. Out of six 3D classes, only one class had clear DNA and streptavidin densities (class #4). This 3D class contained 24% of the "good" raw particles and was used for further refinement, yielding the reported 3D map at 6.1 Å-resolution, according to the gold standard Fourier shell correlation (lower right panel). The streptavidin was flexible and its density was visible only at reduced surface-rendering threshold.

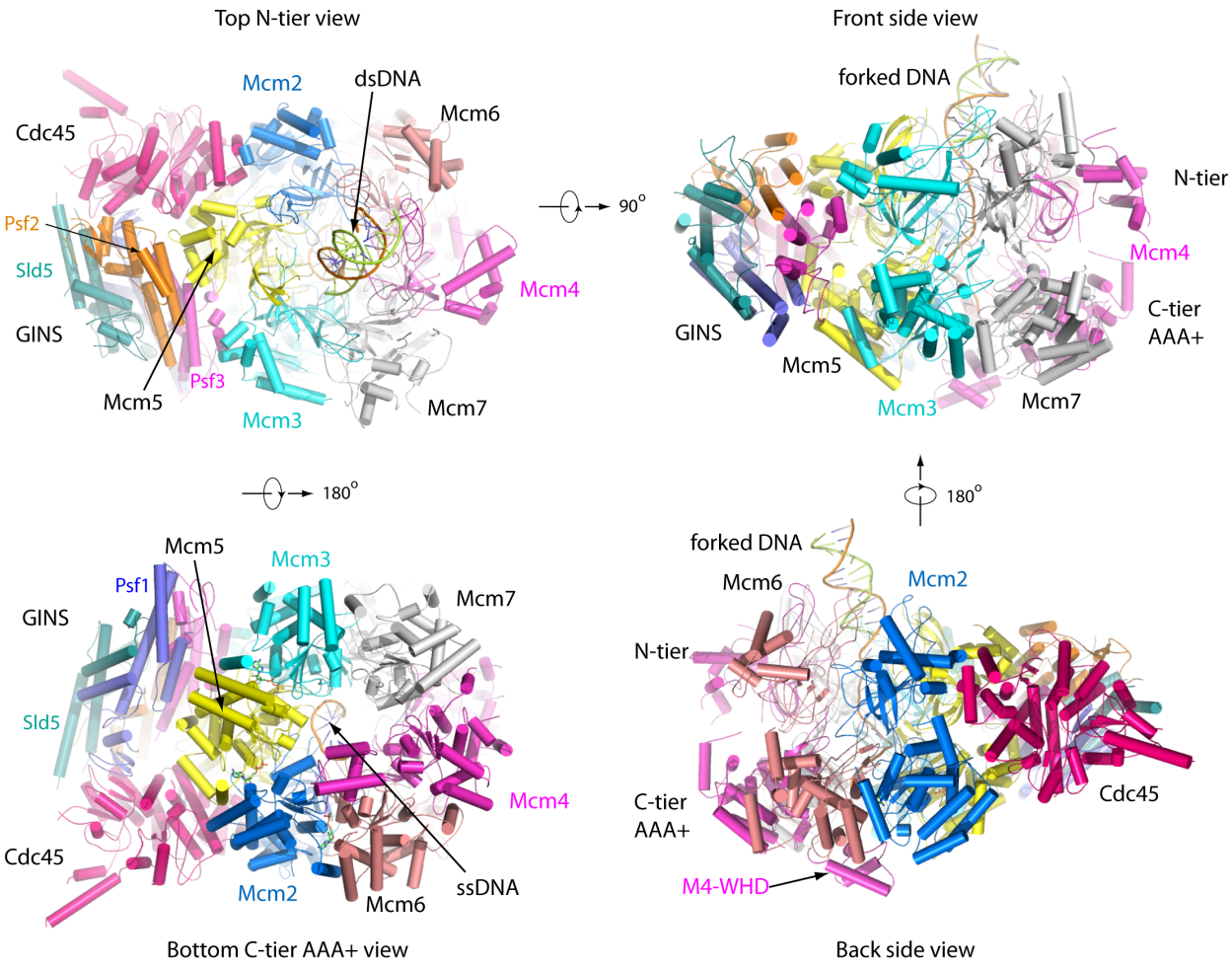

SI Appendix, Figure S10. Overall structure of CMG-forked DNA in cartoon.

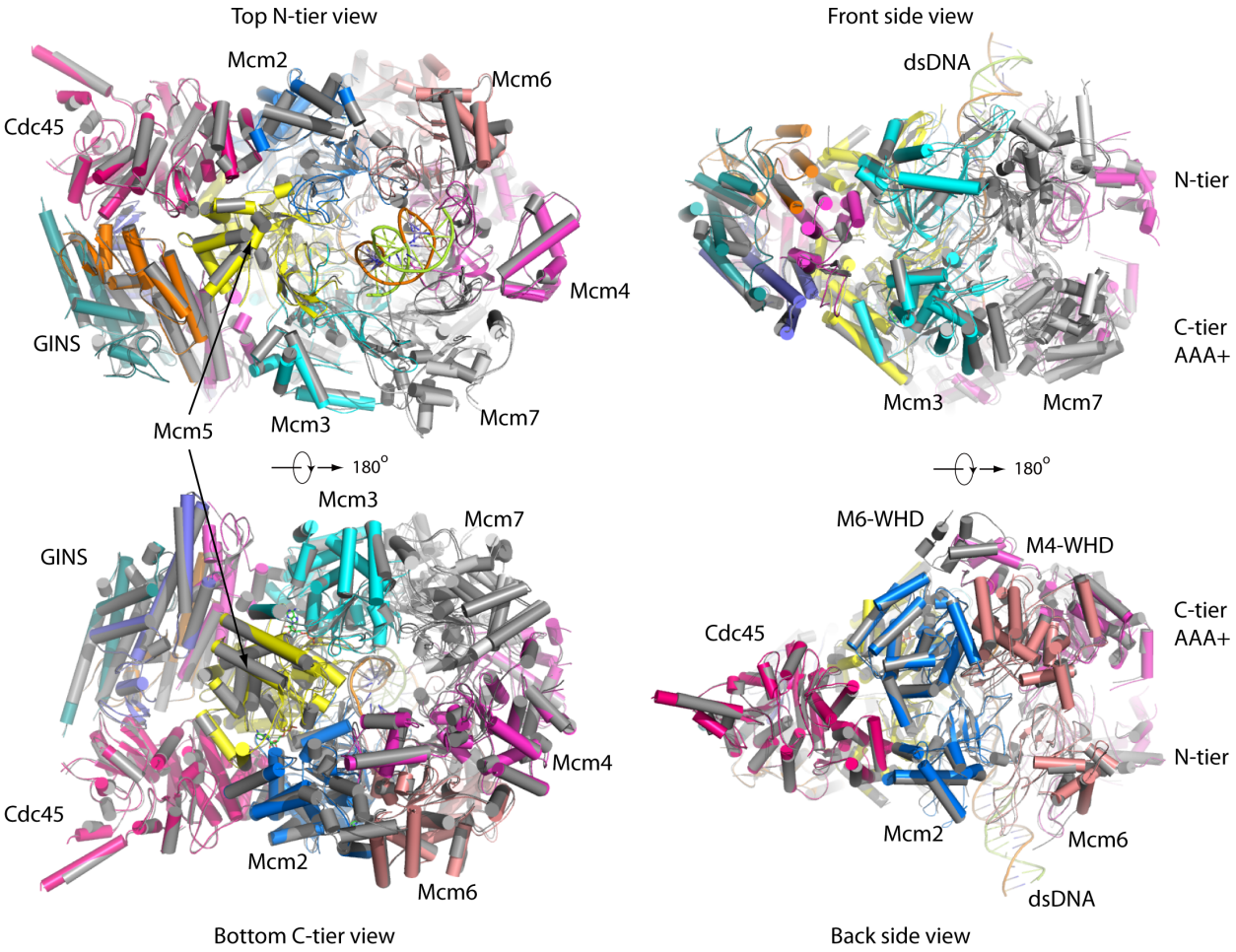

SI Appendix, Figure S11. Superimposition of CMG-ssDNA and CMG-forkDNA reveals high similarity of the two structures, with an RMSD of 1.34 Å.

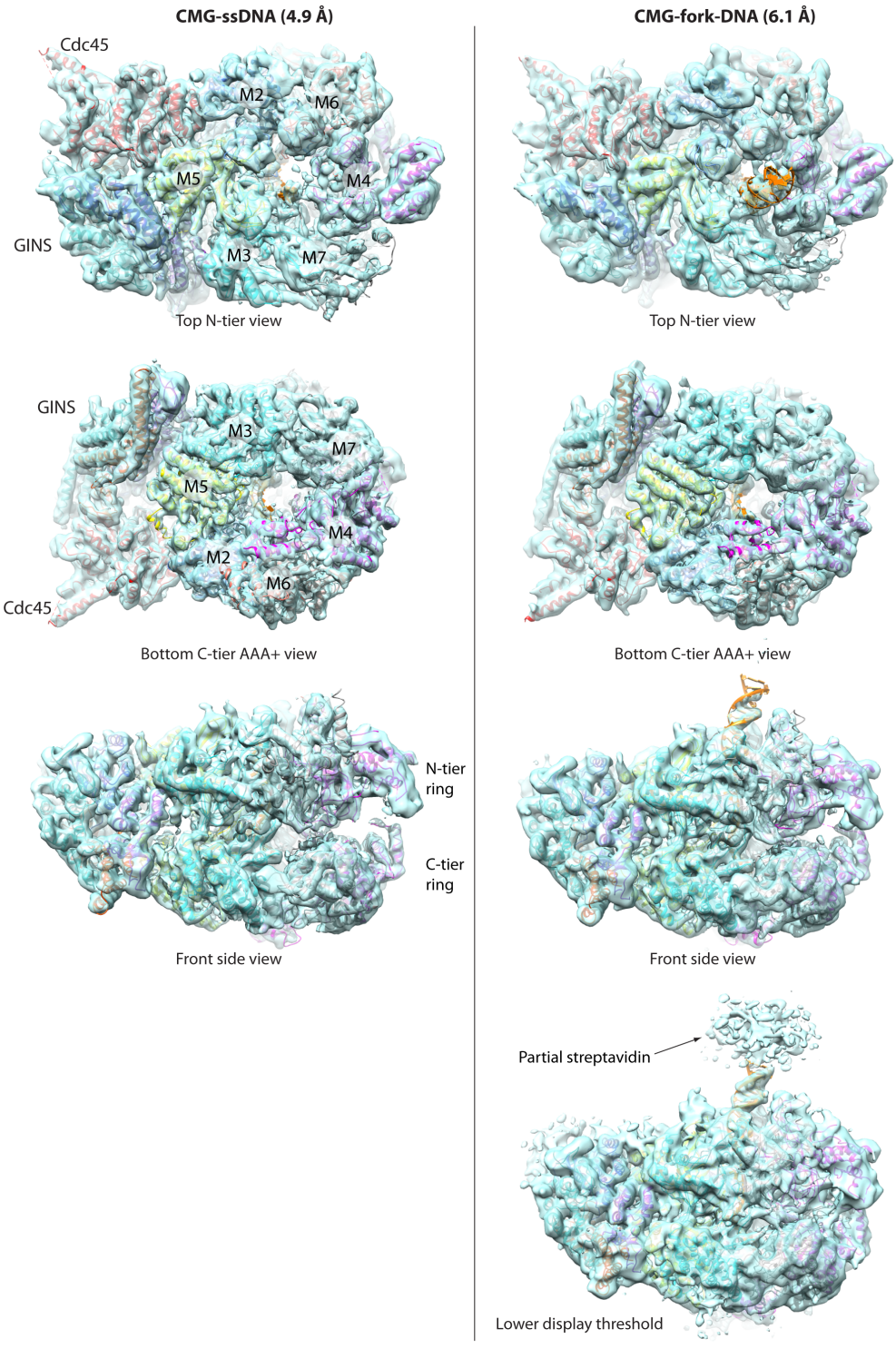

SI Appendix, Figure S12. Comparison of the structure of CMG bound to the forked DNA blocked by streptavidin in the presence of ATP at 6.1 Å resolution (upper panels) with the structure of CMG bound to the ssDNA in the presence of AMPPNP at 4.9 Å resolution (lower panels). The streptavidin density in the CMG-fork DNA 3D map is visible only at a lower surface-rendering threshold.

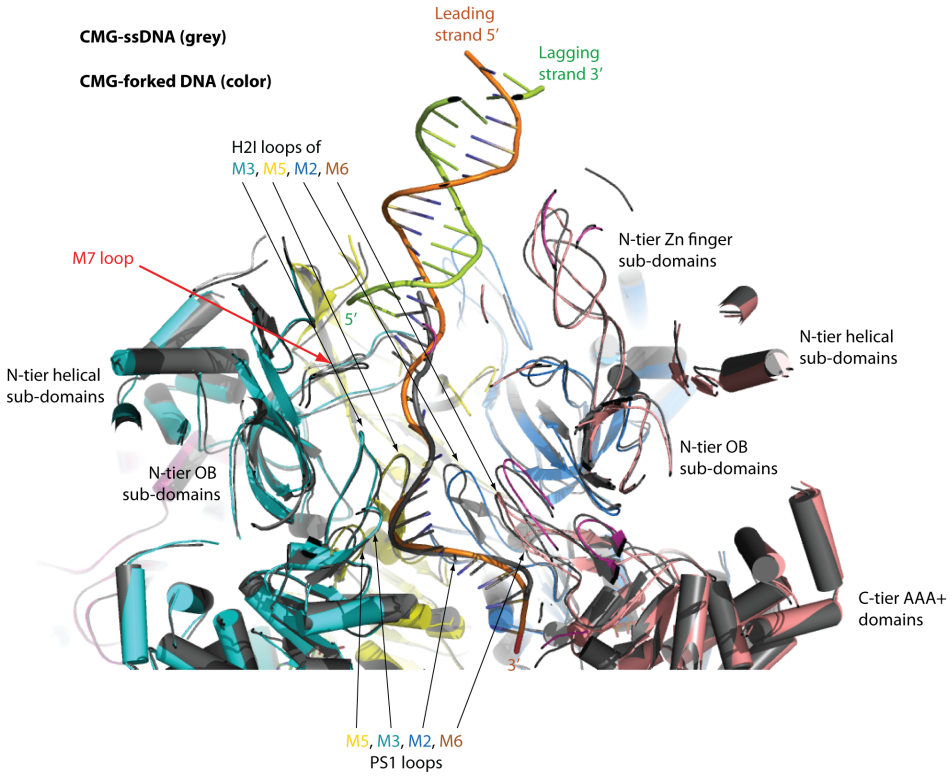

SI Appendix, Figure S13. Superimposition of the CMG-ssDNA structure (grey) and the CMG-forked DNA structure (color). The 14-base ssDNA in the CMG-ssDNA aligns well with the leading strand of the CMG-forked DNA structure. The Mcm7 OB loop projects to the dsDNA-ssDNA junction, appearing to block the lagging strand from further entering the Mcm2-7 central channel.

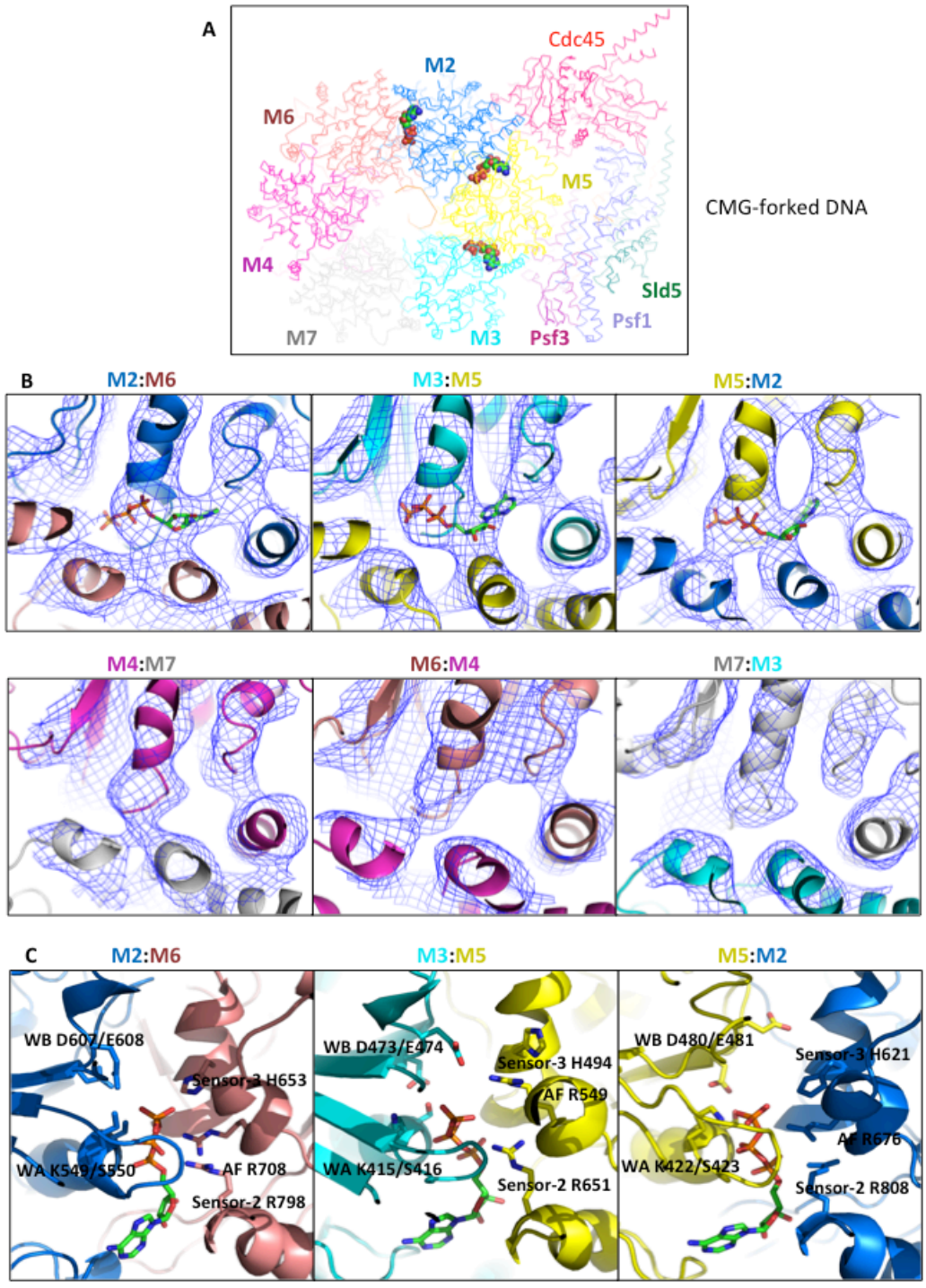

SI Appendix, Figure S14. Nucleotide occupancy in the cryo-EM 3D map of the CMG-forked DNA in the presence of ATP. (**A**) Atomic model of CMG-forked DNA with three modeled AMPPNM at the interfaces between Mcm2-Mcm6, Mcm5:Mcm3, and Mcm5:Mcm2. (**B**) Electron density map around the three bound nucleotides. (**C**) Residues around the bound nucleotides.

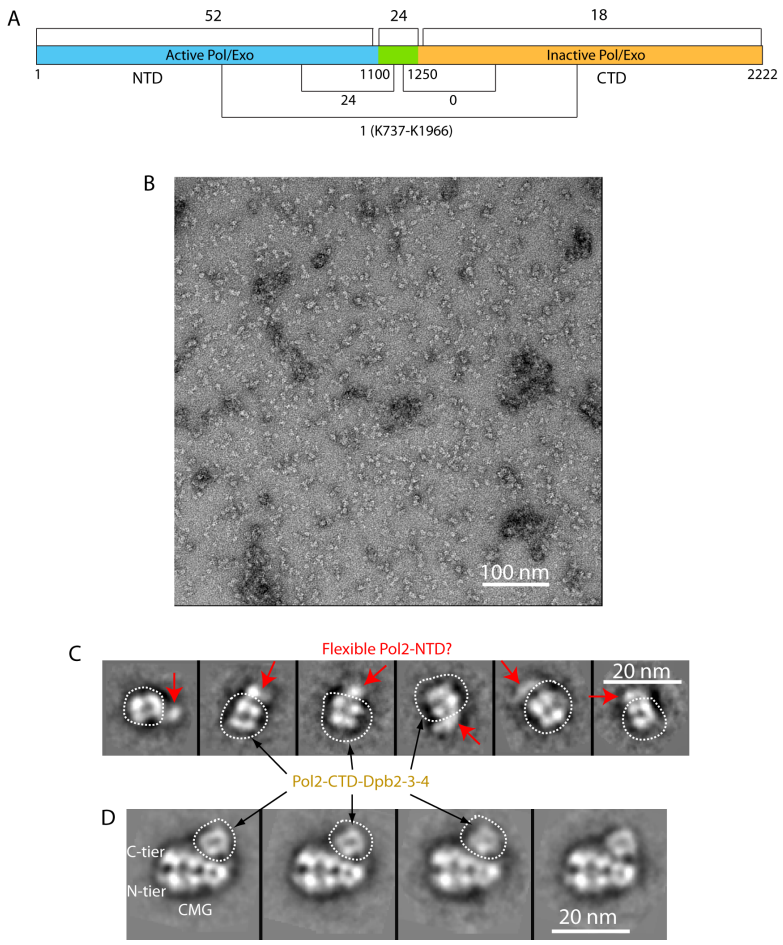

SI Appendix, Figure S15. Cross-linking mass spectrometry and negative stain EM indicates Pol2 is organized into two separate and flexible domains. (**A**) The Pol2 contains an active polymerase in the N-half (light blue) and inactive polymerase in the C-half (orange). The two halves are spatially separate because the active and inactive polymerases contain 52 and 18 intra-molecular cross-links within them, yet there is only one cross-link between the two halves. The green region is an area of many positive charged residues and contains 24 cross-links within itself and 24 cross-links to the N-half, but no cross-links to the C-half. This region of highly positive charged residues may constitute a linker between the two halves of Pol 2. The C-half inactive polymerase binds Dpb2,3,4 [5] and the CX-MS reveals a proximity of the C-half of Pol2 to Psf1, and the CTD of Mcm2 and Mcm6 [6]. Therefore the C-half of Pol2, along with the accessory subunits of Pol ε, is likely the observed density in the EM study [6] that accounts for 70% of the mass of Pol ε, and the N-half of Pol2 may be averaged out in the 3D reconstruction as proposed in Fig. S6b of reference [6]. (**B**) Negative stain image of Pol ε, showing that the particles are widely spaced apart. (**C**) Selected 2D class averages of Pol ε that show a square-like shape (dotted enclosure) that is similar to the shape of the observable portion of Pol ε in side views of 2D averages of CMGE. Note that the encircled square like portion of Pol ε. (**D**) Side-views of 2D averages of CMGE from ref [6]. The observable portion of Pol ε in CMGE is encircled in the left 3 panels.

References

1. Abid Ali F et al. (2016) Cryo-EM structures of the eukaryotic replicative helicase bound to a translocation substrate. *Nat Commun* 7: 10708. doi: 10.1038/ncomms10708.

2. Enemark EJ and Joshua-Tor L (2006) Mechanism of DNA translocation in a replicative hexameric helicase. *Nature* 442(7100): 270-275.

3. Thomsen ND and Berger JM (2009) Running in reverse: the structural basis for translocation polarity in hexameric helicases. *Cell* 139(3): 523-534.

4. Itsathitphaisarn O, Wing RA, Eliason WK, Wang J and Steitz TA (2012) The hexamer helicase DnaB adopts a nonplanar conformation during translocation. *Cell* 151(2): 267-277.

5. Pursell ZF, Kunkel TA (2008) DNA polymerase epsilon: a polymerase of unusual size (and complexity). Prog Nucleic Acid Res Mol Biol. 82:101-45.

6. Sun J et al. (2015) The Architecture of a Eukaryotic Replisome. *Nat Struct Mol Biol* 22(12): 976-982.